Wave propagation in birefringent materials with off-axis absorption or gain

Mahmood Sabooni,[1,2,*] Adam N. Nilsson,[2] Gerhard Kristensson,[3] and Lars Rippe[2]

[1]*Department of Physics, University of Tehran, 14399-55961, Tehran, Iran*
[2]*Department of Physics, Lund University, P.O. Box 118, SE-22100 Lund, Sweden*
[3]*Department of Electrical and Information Technology, Lund University, P.O. Box 118, SE-22100 Lund, Sweden*

The polarization direction of an electromagnetic field changes and eventually reaches a steady state when propagating through a birefringent material with off-axis absorption or gain. The steady state orientation direction depends on the magnitude of the absorption (gain) and the phase retardation rate. The change in the polarization direction is experimentally demonstrated in weakly doped (0.05%) $Pr^{3+} : Y_2SiO_5$ crystals, where the light polarization, if initially aligned along the most strongly absorbing principal axis, gradually switches to a much less absorbing polarization state during the propagation. This means that the absorption coefficient α in birefringent materials generally varies with length. This is important for, e.g., laser crystal gain media, highly absorbing and narrow band spectral filters and quantum memories.

I. INTRODUCTION

For electromagnetic plane wave propagation in birefringent materials the instantaneous polarization direction of the electric field vector **E** normally changes during the propagation. For example, the polarization of a wave propagating along one of the principal axes in a (nonabsorbing) birefringent material with (initially) linear polarization at an angle γ relative to one of the other principal axes, changes from linear to elliptical (with major axes $|\mathbf{E}| \cos\gamma$ or $|\mathbf{E}| \sin\gamma$) and then to linear polarization at angle $-\gamma$ and then back to elliptical, etc. as it propagates through the material. For a case where the wave is not propagating along one of the principal axes the wave vector and the Poynting vector are in general not parallel and there are walk-off effects (e.g., Chap. 6 in Ref. [1]).

In this work we consider an initially linearly polarized plane wave, propagating along a principal axis in a nonmagnetic off-axis absorbing birefringent material. In this case polarization rotation can occur even if the initial linear polarization is aligned with one of the principal axes. In materials with absorption or gain the development of the polarization can be complicated. Not only could there be oscillations between linear and elliptical polarization and walk-off effects, there can also be conversions from light of one polarization to another polarization due to the absorption (or gain).

Such effects should for example be present in laser crystal gain media when the gain is anisotropic and the gain tensor is not aligned with the principal axes [2]. Recently there has also been an interest in highly absorbing and very narrow bandwidth filters for very specific applications such as quantum memories [3], or highly absorbing narrow-band filters with exceptionally large etendue [4,5] for high performance ultrasound optical tomography [5,6] and also dynamically tunable high performance filters [7]. All these recent papers use filters based on rare-earth–ion-doped inorganic crystals where the absorption tensor is not aligned with the principal axes. As a consequence the light polarization gradually switches during propagation to a much less absorbing polarization state

even if the input polarization is perfectly aligned with the most strongly absorbing principal axis. This significantly decreases the achievable filter attenuation from what might be anticipated based on just the material absorption coefficient.

In this work we theoretically analyze the polarization rotation in absorbing birefringent materials with a model adapted from [8]. We provide some simple relations of when the effects need to be taken into account and give possible suggestions on how to maintain the original high absorption. The theoretical analysis is supported by an experimental demonstration of the polarization rotation effect.

The paper is organized as follows. First an intuitive theoretical background is given. This is followed by simulation results and discussions of polarization steady states and the effects of absorption on light propagating through a crystal. Experimental results are then presented where the incoming and outgoing polarization directions are studied for crystals with different absorption and length. Lastly a remark about the maximum absorption axis is made before the paper is concluded with a summary. A rigorous mathematical treatment of the problem can be found in the Appendixes.

II. THEORETICAL BACKGROUND

A detailed description of the theoretical framework is given in the Appendixes, but a simple and intuitive understanding can be achieved by considering the effects of birefringence and absorption separately. In Fig. 1(a) we see the principal axes of a birefringent crystal as well as the direction of the transition dipole moment $\boldsymbol{\mu}$. This direction does not coincide with any of the principal axes of the crystal. An incoming plane wave $\mathbf{E}_{in}$, which is on resonance with the absorbing transition and with its polarization oriented along one of the principal axes D_2, generates a polarization **P** along $\boldsymbol{\mu}$ with a 90° phase shift. This polarization generates a field $\mathbf{E}_P$ along $\boldsymbol{\mu}$ with a relative phase relation to $\mathbf{E}_{in}$ [9,10] as shown in Fig. 1(b). The total resulting electromagnetic field $\mathbf{E}_{tot} = \mathbf{E}_{in} + \mathbf{E}_P$ now also have a component along the D_1 axis as shown in Fig. 1(c). Since the crystal is birefringent the polarization state oscillates between linear [Figs. 1(c) and 1(e)] and elliptical [Fig. 1(d)] as the field propagates through

---
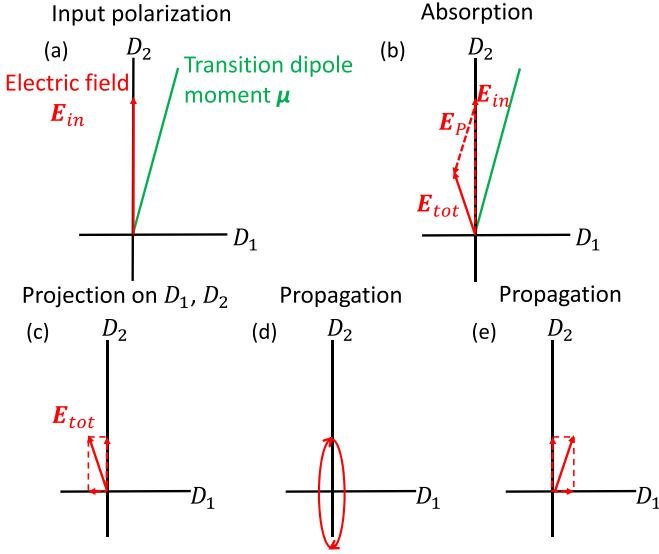*m.sabooni@ut.ac.ir; mahmood.sabooni@fysik.lth.se

FIG. 1. Simplified view of the propagation of an electric field through a birefringent crystal with a transition dipole moment axis tilted with respect to the crystal axes ($D_1 \perp D_2$). (a) The incoming electric field $\mathbf{E}_{in}$ is polarized along D_2. (b) The material is polarized by the incoming plane wave and emits an electric field $\mathbf{E}_P$ along the transition dipole moment which is 180° out of phase with the incoming field $\mathbf{E}_{in}$ [9,10], resulting in the total field $\mathbf{E}_{tot} = \mathbf{E}_{in} + \mathbf{E}_P$ which has both a D_1 and D_2 component of the electric field. The magnitude of $\mathbf{E}_P$ is exaggerated to make the effects easier to see. The electric field is projected along the crystal axes D_1 and D_2 in (c) to make it possible to see the effect of propagation through the birefringent crystal which causes a relative phase change between the two electric field components. In (c) they are oscillating in phase, while in (d) they are 90° out of phase and in (e) they are completely out of phase (180°).

the crystal. Of course in reality the effects of absorption and birefringence are intertwined and occur simultaneously. The theoretical examination in the Appendixes makes it possible to simulate the propagation of any incoming electric field polarization through a birefringent crystal with an absorption axis with an angle to the principal axes, a problem that cannot be trivially solved by choosing a new coordinate basis. Our method works for infinite incoming plane waves and assumes that the lateral (transverse) dimensions of the crystal are infinite as well. Discussions around the results from these simulations can be found in the next section.

III. SIMULATION RESULTS

In this section results from simulations of light propagation inside a birefringent crystal with a tilted transition dipole moment direction is analyzed. As a specific example a 0.05% $Pr^{3+} : Y_2SiO_5$ crystal is chosen where the transition dipole moment is tilted by $74.6 \pm 1.9°$ from the D_1 crystal axis [11] as seen in Fig. 2 and calculated in the Appendixes, see Eq. (B18).

A. Phase retardation in a birefringent crystal

The propagation phase ϕ can be written as $\phi = 2\pi \frac{nz}{\lambda_0}$ rad, i.e., light with the wavelength λ_0 in vacuum experiences a
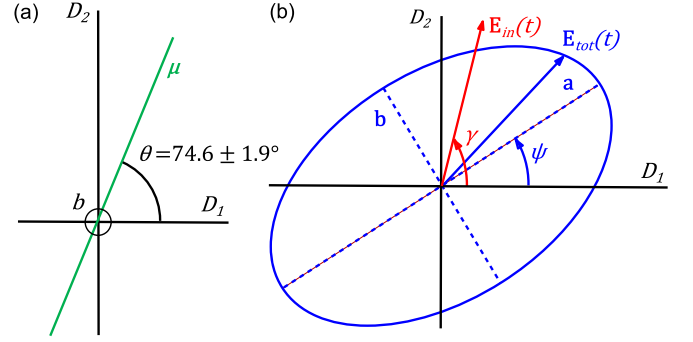

FIG. 2. (a) Transition dipole moment $\boldsymbol{\mu}$ versus principal axes for $Pr^{3+} : Y_2SiO_5$ ($D_1 \perp D_2 \perp b$). (b) Notation of linear incoming and elliptical outgoing polarizations are seen where γ is the angle between the D_1 axis and the incoming polarization and ψ is the angle between the D_1 axis and the major axis **a** of the outgoing elliptical polarization.

phase shift of ϕ rad when traveling an optical length nz through a material, where n is the index of refraction and z is the propagation depth. The difference between the accumulated phases ϕ_2 and ϕ_1 for light propagating along two different crystal axes D_2 and D_1, respectively, is termed the phase retardation

$$\Delta\phi = \phi_2 - \phi_1 = 2\pi \frac{\Delta nz}{\lambda_0}, \quad (1)$$

where $\Delta n = n_{(D_2)} - n_{(D_1)}$. The crystal length needed to obtain a quarter-wave plate $\Delta\phi = \frac{\pi}{2}$ for a Y_2SiO_5 crystal with the different refractive indices $n_{(D_1)} = 1.7881$, $n_{(D_2)} = 1.809$, and $n_b = 1.7851$ along the principal axes [12] is calculated using Eq. (1) to be about 7.25 μm for light propagating along the b axis.

B. Polarization steady states

From the effects explained in Fig. 1 it is clear that it is not possible to maintain a pure linear polarization when propagating through a crystal where the transition dipole moment axis does not coincide with any of the optical axes of the crystal. However, in general two steady state polarization solutions exist for a forward propagating wave. They are elliptically polarized and only differ by a 90° rotation of their major axes in the D_1-D_2 plane. The polarization of the steady state does not change when propagating through the crystal. The ellipticity and the direction of these polarizations depend on the following ratio:

$$R = \frac{n_{(D_2)}^2 - n_{(D_1)}^2}{\chi_{abs}}, \quad (2)$$

where χ_{abs} is the electric susceptibility connected to the absorption [for $Pr^{3+} : Y_2SiO_5$ see Eq. (A16)]. In general, only the steady state solution with the lowest absorption or highest gain is stable.

In Figs. 3(a)–3(c) the steady state polarization solutions when the transition dipole moment makes an angle of 74.6° relative to the D_1 axis are shown for three different cases where $R \gg 1$, $R \approx 1$, and $R \ll 1$, respectively. For absorption the green curves are stable solutions and the red curves are unstable. The reverse is true in the case of gain. The first
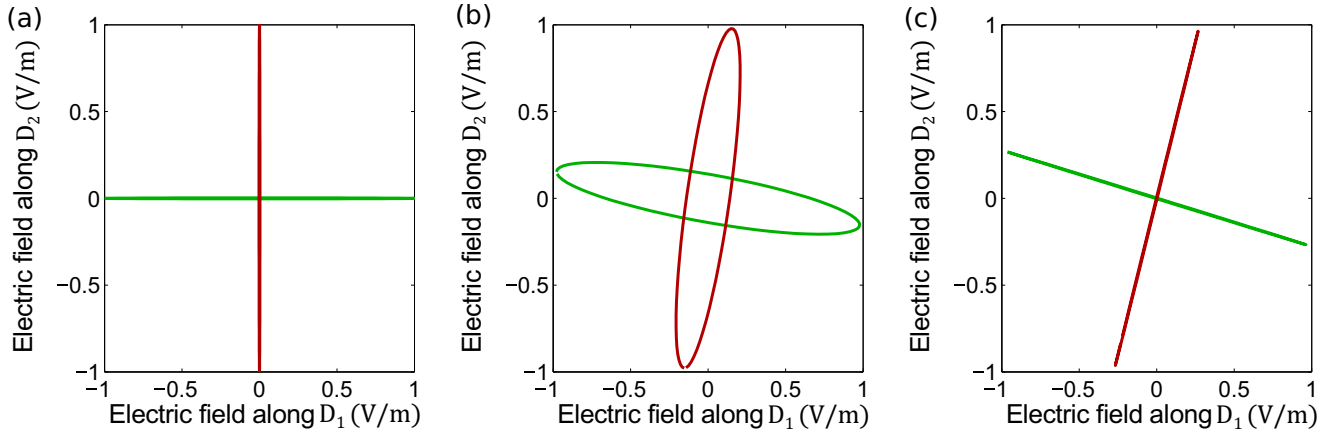
FIG. 3. Polarization steady states for (a) $Pr^{3+} : Y_2SiO_5$ with absorption coefficients $\alpha_{D_1} = 3.6 \pm 0.5$ cm^{-1} and $\alpha_{D_2} = 47 \pm 5$ cm^{-1} which corresponds to an absorption susceptibility $\chi_{abs} = (8.82 \pm 0.8) \times 10^{-4}$ and a transition dipole moment direction with an angle $\theta = 74.6 \pm 1.9°$ from D_1 as can be seen in Fig. 2(a). (b) and (c) Increased absorption susceptibility χ_{abs} by a factor of 100 and 10 000, respectively. The ratio R in Eq. (2) is (a) $R \approx 85$, (b) $R \approx 0.85$, and (c) $R \approx 0.0085$. The green curves are stable (unstable) and the red curves are unstable (stable) in the case of absorption (gain).

case, seen in Fig. 3(a), is the same as for a 0.05% $Pr^{3+} :$ Y_2SiO_5 crystal which has a transition dipole moment direction that is tilted $74.6 \pm 1.9°$ from D_1 and absorption coefficients along D_1 and D_2 of $\alpha_{D_1} = 3.6 \pm 0.5$ cm^{-1} and $\alpha_{D_2} = 47 \pm 5$ cm^{-1} which corresponds to an electric susceptibility for the absorption that is $\chi_{abs} = (8.82 \pm 0.8) \times 10^{-4}$. The difference $n_{(D_2)}^2 - n_{(D_1)}^2$ in Y_2SiO_5 is 0.075, which gives a ratio $R \approx 85 \gg 1$. Here one can see that the steady state solutions lie, respectively, along the D_1 and the D_2 crystal axes, which is always the case for $R \gg 1$.

The next two cases seen in Figs. 3(b) and 3(c) use the same values mentioned above except that the absorption susceptibility χ_{abs} is increased by a factor 100 and 10 000, respectively. In the extreme where $R \ll 1$, seen in Fig. 3(c), the solutions lies almost completely along the transition dipole moment (unstable for absorption) and perpendicular to it (stable for absorption). In between these extreme cases when $R \approx 1$, seen in Fig. 3(b), the solutions lie between the crystal axes and the transition dipole moments and have a higher ellipticity than in the extremes.

The steady state solutions can be explained by the same phenomena that was discussed in Fig. 1, i.e., that an electric field in D_2 creates an electric field in D_1, and vice versa, due to the tilted absorption (gain) axis. The steady state solutions are polarization states where the sum of the components lost and absorbed in D_1 decays at the same rate as the sum of the components created and absorbed along D_2, which in other words means that the polarization stays the same.

The dependence on R can be intuitively explained by rewriting the numerator in Eq. (2) as

$$n_{(D_2)}^2 - n_{(D_1)}^2 = \left(n_{(D_2)} + n_{(D_1)}\right)\left(n_{(D_2)} - n_{(D_1)}\right)$$
$$= \left(n_{(D_1)} + n_{(D_1)}\right)\Delta n. \qquad (3)$$

If we now assume that $n_{(D_1)}$ and $n_{(D_2)}$ are roughly constant then the ratio R measures if Δn is small or large compared to the absorption and Δn sets the rate at which phase retardation

is accumulated [see Eq. (1)]. In other words if $R \gg 1$ then the phase retardation dominates over the absorption. This makes all polarizations that are symmetric along the crystal axes equivalent [due to the effects explained in Figs. 1(c)–1(e)] and therefore the only steady state solutions that can exist are along D_1 and D_2, see Fig. 3(a). In the other extreme where $R \ll 1$ the absorption dominates and any phase retardation between the two electric field components can be ignored, which leads to one solution orthogonal and one solution parallel to the transition dipole moment axis, see Fig. 3(c).

C. Electric field absorption when $R \gg 1$

From the simulations one can obtain the (expected) exponential decay in the electric field components along D_1 and D_2 as a function of propagation. For the example of $Pr^{3+} : Y_2SiO_5$ the decay coefficients can be seen in Fig. 4(a) for a linear input polarization along D_2 [$\gamma = 90°$ in Fig. 2(b)]. Even though the input polarization only has a D_2 component of the electric field, a D_1 component is almost immediately created in the crystal due to the effects explained in Figs. 1(a) and 1(b). Since this effect is dual, i.e., a D_2 component creates a small D_1 component and vice versa, the net effect will be that the largest component creates a smaller orthogonal component. Therefore, the relative size of the created component is the same as the ratio of the D_2 and D_1 component of the steady state, since at the steady state (when the polarization no longer changes with propagation) the D_2 component is almost completely created by the tilted absorption of the D_1 component. Therefore, it is a measure of how strong the connection between the two components is. For the case of $Pr^{3+} : Y_2SiO_5$ the initial electric field component along D_1 is approximately a factor of 330 less than the D_2 component [see Fig. 4(a) and Eq. (B9)].

The exponential decay along D_2 is much larger than along D_1 in the beginning of the propagation due to the fact that the transition dipole moment lies much closer to D_2. However
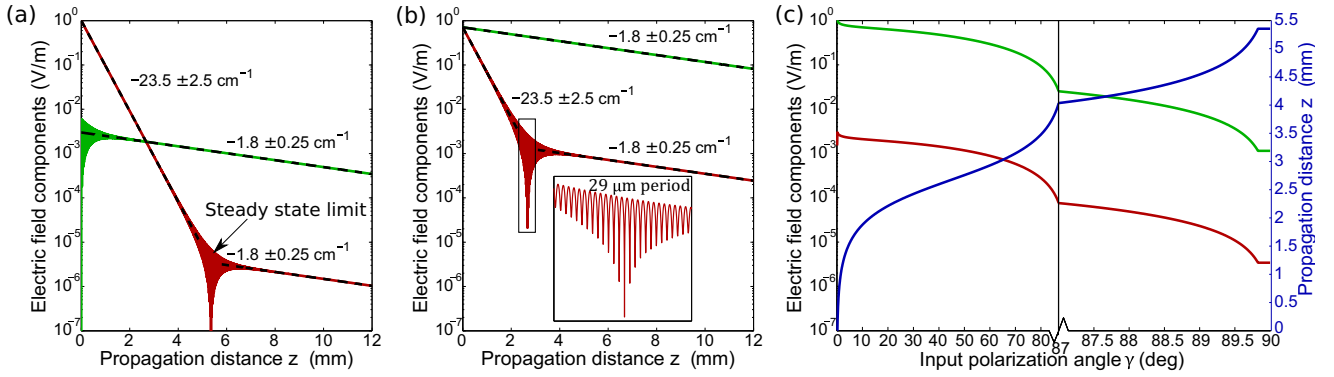
FIG. 4. Shows the decay of the electric field components along crystal axes D_1 (green) and D_2 (red) as a function of propagation distance z for a linear input polarization at an angle (a) $\gamma = 90°$ and (b) $\gamma = 45°$ from D_1. The dashed black lines are linear fits to the logarithm of the electric field in the form $\ln[E(z)] = \ln(E_0) + Cz$, where the value of C is displayed next to each black curve. Note that these values represent the decay of the electric field. To obtain the absorption coefficients for the intensity multiply these values with 2, i.e., $\alpha_{D_1} = 3.6 \pm 0.5$ cm^{-1} and $\alpha_{D_2} = 47 \pm 5$ cm^{-1}. The steady state limit can be seen in (a) which shows the largest total absorption that can be reached with a high absorption rate for a linear polarization. The inset in (b) is a zoomed in view of the steady state limit reached after ≈ 2.7 mm for $\gamma = 45°$. The oscillating pattern has a period of 29 μm (matching a 2π phase evolution calculated with Eq. (1) and exists due to the interactions between the polarization induced in the material and the electric field of the light and the birefringence of the crystal. (c) The (approximate) propagation distance needed to reach the steady state limit shown in blue as a function of the input polarization angle γ together with the electric field component along D_1 (green) and along D_2 (red) at the steady state limit. Note that the x axis is cut at 87° and that the axis scale changes afterwards. Note also the plateau reached at 89.83° which shows that better angle precision than that is not needed.

towards the end of the propagation the stable steady state solution is reached and both components decay at the same rate. Continuing in Fig. 4(b) the input polarization is changed to $\gamma = 45°$ and the polarization steady state is reached sooner since the input polarization is more similar to the stable steady state. For a linear input polarization the highest absorption rate is achieved along D_2 but slows down after propagating around 5.4 mm, see Fig. 4(a). This leaves us with the ultimate limit, which we call the "steady state limit," of the maximum electric field absorption with a high absorption rate of the incoming light for this material to be 10^{-6}–10^{-5} and this is reached for a 5.4-mm-long crystal. To clarify, the light continues to be absorbed after this limit but at a much slower rate. In light of this limit it is clear that scaling a crystal longer than ≈ 5.4 mm to gain absorption serves limited purpose and one can get exponentially higher absorption by avoiding the steady state limit. Note also that much earlier, at around 2.7 mm, the electric field component along D_1, which decays much slower, is of the same size as the component along D_2 and the D_1 component dominates after 2.7 mm, even though the D_1 component was zero before entering the crystal, this component can however be blocked with a polarizer after the crystal.

The (approximate) propagation distance needed to reach the steady state limit as a function of the input polarization γ is shown in blue in Fig. 4(c). The electric field component along D_1 and D_2 when the steady state limit is reached is also shown in green and red, respectively. Note that the D_1 electric field component is always a factor of ≈ 330 larger than the D_2 component when the steady state solution is reached. Close to $\gamma = 90°$ the propagation distance decreases quite rapidly as γ departs from 90°. Therefore, high polarization purity is required to have a high absorption and a steady state limit at 5.4 mm. The polarization purity is defined as the ratio of the desired and undesired polarization component, in this case the ratio of the D_2 and the D_1 component. The purity

needed is in the order of the ratio of the D_2 and D_1 electric field components for the stable steady state; higher purity is unnecessary since a small D_1 component of this size will be created during the first few μm of propagation. For Pr^{3+} : Y_2SiO_5, seen in Fig. 3(a), this ratio is ≈ 330 for the electric field, or equivalently 10^5 for the intensity components [see Eq. (B9)]. This means that a polarizer with a suppression of 10^5 and a polarization angle precision of around 0.17° is required to achieve the longest propagation distance with maximum absorption.

To avoid the steady state limit one has to suppress the D_1 component of the light. This can be done with, e.g., a linear polarizer. To achieve high absorption it is therefore better to use several smaller crystals (lengths of $\leqslant 5.4$ mm) with linear polarizers blocking any D_1 component in between each set of crystals instead of using one long crystal.

IV. EXPERIMENTAL RESULTS

To examine the polarization change during propagation several experiments were performed on crystals with different lengths. We used three 0.05% Pr^{3+} : Y_2SiO_5 crystals with different lengths (1, 6, and 12 mm) and measured the outgoing polarization direction ψ as a function of the incoming polarization angle γ, see Fig. 2(b). The crystals were kept at cryogenic temperature (2 K). The setup is illustrated in Fig. 5(a). The absorption was probed with attenuated pulses to minimize saturation effects on the absorption and between each experiment a set of hole eraser pulses were used over a wide spectral range to make sure that no permanent hole burning occurred.

According to the simulations for a Pr^{3+} : Y_2SiO_5 crystal there is a minimum (sufficient) value of the absorption where the steady state solution is reached which means that the outgoing polarization is almost entirely along the D_1 axis.
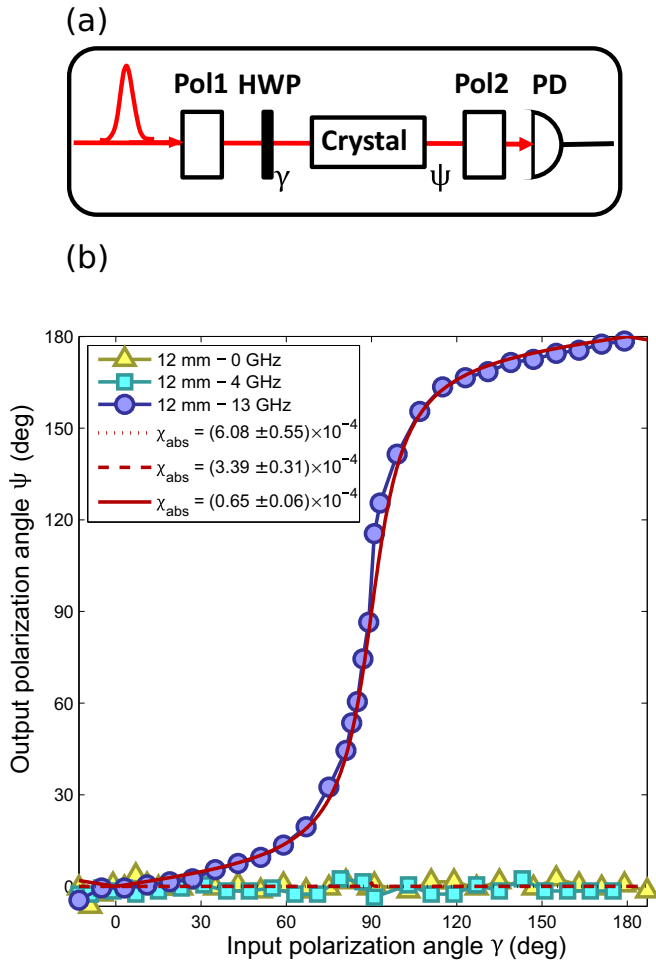
(a)

(b)

FIG. 5. (a) Polarization analyzer setup. First, two polarizers are calibrated against each other by minimizing the photodiode (PD) signal when there is nothing in between them. The first polarizer (Pol1) and the half-wave plate (HWP) makes sure that the incoming linearly polarized light is at an angle γ from D_1. The D_1 and D_2 directions are measured with the same setup with the crystal at room temperature where absorption is negligible. By turning the second polarizer (Pol2) to maximize the throughput to the photodiode (PD) the outgoing polarization after the crystal is measured to be ψ. (b) Three experiments were performed on a 12 mm crystal 0, 4, and 13 GHz away from the center of the inhomogeneous absorption profile. The simulations have $\chi_{\rm abs}$ given by Eq. (4) which assumes an inhomogeneous profile in the shape of a Lorentzian distribution using a FWHM of 9 GHz, which was measured in the experiment. The experimental results are displayed as yellow triangles, cyan squares, and blue dots together with a red dotted, dashed, and solid curve, respectively, for the three cases of 0, 4, and 13 GHz. Note that the simulation results for the 0 and 4 GHz cases overlap.

A 12 mm Pr^{3+} : Y_2SiO_5 crystal is employed to illustrate this effect as shown in Fig. 5(b), where three measurements at different frequencies within the inhomogeneous profile were performed. The inhomogeneous linewidth Γ of this crystal is measured to be about 9 GHz. The three sets of measurements at frequencies 0, 4, and 13 GHz relative to the line center are shown in Fig. 5(b) as yellow triangles, cyan squares, and blue dots, respectively, together with simulations for each case

displayed as a red dotted, dashed, and solid curve. For high and intermediate absorption the outgoing polarization is along the D_1 axis which agrees with the fact that the D_2 component is absorbed much quicker than the D_1 component.

As shown in Figs. 1(c)–1(e) the outgoing polarization shifts significantly during propagation. It is therefore impossible to determine if the outgoing polarization is in the range $\psi = 0°$–$90°$ or $\psi = 90°$–$180°$ for a given input polarization without a very precise knowledge of the crystal length. A quarter-wave plate distance was calculated previously to be $L \approx 7.25$ μm which means that a full evolution of the phase is done in ≈ 29 μm in Y_2SiO_5. If the crystal length is not known within this precision it is indeed impossible to determine the outgoing polarization direction. The crystal length used in the simulations is therefore changed from exactly 12 mm by a few tens of μm to the value that best matches the experimental results.

The absorption coefficients in [11] are measured in a crystal with a linewidth of $\Gamma = 6.2$ GHz and which nominally has the same Pr concentration, 0.05% as in the present crystal. This would correspond to a peak absorption susceptibility of $\chi_{\rm abs}^{\rm peak} = (8.82 \pm 0.8) \times 10^{-4}$. The inhomogeneous profile can be approximated as a Lorentzian profile [11] that in our experiments have a linewidth of $\Gamma = 9$ GHz. Assuming that the integral of the absorption should be the same for our crystal and the crystal used in [11] the peak absorption susceptibility of our crystal should be reduced by a factor 9/6.2 which gives $\chi_{\rm abs}^{\rm peak} = (6.08 \pm 0.55) \times 10^{-4}$. Since the three measurements seen in Fig. 5(b) are performed at different positions on the inhomogeneous profile the absorption susceptibility used in the simulations must be adjusted accordingly:

$$\chi_{\rm abs} = \chi_{\rm abs}^{\rm peak} \frac{(\Gamma/2)^2}{(f - f_0)^2 + (\Gamma/2)^2},$$
$$\chi_{\rm abs,1} = [f - f_0 = 0 \text{ GHz}] \approx (6.08 \pm 0.55) \times 10^{-4},$$
$$\chi_{\rm abs,2} = [f - f_0 = 4 \text{ GHz}] \approx (3.39 \pm 0.31) \times 10^{-4}, \quad (4)$$
$$\chi_{\rm abs,3} = [f - f_0 = 13 \text{ GHz}] \approx (0.65 \pm 0.06) \times 10^{-4}.$$

The simulations agree well with the experimental results and only in the 13 GHz case is the absorption so low that the outgoing polarization varies from D_1. The results from the 1 and 6 mm crystals give similar results that agree with the simulations. Also here the absorption susceptibility must be reduced with respect to the peak value to account for the experiments taking place at the side of the inhomogeneous profile.

V. MAXIMUM ABSORPTION AXIS

It has previously been shown, see Ref. [13], that slow light effects split an incoming linear polarization into two parts, where one part has a significantly larger slow light effect than the other. The transition dipole moment direction was then considered as the maximum absorption direction but it turns out that the maximum (minimum) absorption and consequently time delay happens when we set the input polarization along the D_2 (D_1) axis. In general this depends on the ratio R in Eq. (2), since if $R \ll 1$ the maximum absorption direction is almost exactly along the transition dipole moment axis, but as stated this is not the case for Pr^{3+} : Y_2SiO_5 where $R \approx 85 \gg 1$.

VI. CONCLUSION

In conclusion, we have modeled and analyzed the polarization of light propagating through an absorbing (amplifying) birefringent crystal. Steady state solutions for the polarization of a propagating wave were found and discussed. This led to the conclusion that only increasing the length of a birefringent medium (e.g., a rare-earth–ion-doped crystal) is not the most efficient method to reach higher absorption. This can be an important issue in applications like quantum memories and spectral filtering employing birefringent crystals [3–7]. Since the model works for any birefringent material with either absorption or amplification it can be useful in other applications such as laser crystal gain media or with other materials that are not specifically discussed here.

It also became clear that the polarization direction with maximum absorption (gain) depends upon the ratio between the phase retardation and the magnitude of the absorption (gain). For an absorbing $Pr^{3+} : Y_2SiO_5$ crystal the maximum absorption axis is along D_2, while the stable polarization steady state solution is almost completely along D_1.

This work will hopefully open up new opportunities to investigate more interesting physics and applications regarding the propagation effects in rare-earth–ion-doped crystals in the future.

APPENDIX A

1. Light propagation in a birefringent crystal

The propagation of an electromagnetic field in a general material containing absorption can be a quite complex problem to solve due to the interaction of light and matter, but one could reduce this complexity without losing the generality of the solution by considering a simplification based on the properties of the medium. We start the simplification by considering a plane-stratified medium, which is a valid assumption for the materials investigated in our case. The assumption of plane-stratified media is a proper approximation for materials that show variation in the propagation direction (z axis) but no variation in the lateral (x-y plane) direction. In other words, we have homogeneity (same absorption or gain) in the x-y plane and possible inhomogeneity (varying absorption or gain) along the z axis. The main theoretical concept of the calculations in this paper is discussed with more details in Ref. [8].

For macroscopic media, Maxwell's equations describe the dynamics of the fields as follows (the harmonic time

convention $e^{-i\omega t}$ is used):

$$\nabla \times \mathbf{E}(\mathbf{r},\omega) = ik_0[c_0\mathbf{B}(\mathbf{r},\omega)],$$
$$\nabla \times \eta_0\mathbf{H}(\mathbf{r},\omega) = -ik_0[c_0\eta_0\mathbf{D}(\mathbf{r},\omega)], \quad \text{(A1)}$$

where $\eta_0 = \sqrt{\frac{\mu_0}{\epsilon_0}}$ is the intrinsic impedance of vacuum, and $c_0 = 1/\sqrt{\epsilon_0\mu_0}$ and k_0 are the speed and wave number of light in vacuum, respectively. In addition, $\mathbf{E}$, $\mathbf{B}$, $\mathbf{H}$, and $\mathbf{D}$ are the electric field, magnetic flux density, magnetic field, and the electric flux density, respectively.

In order to apply Maxwell's macroscopic equations, it is necessary to specify the relations between $\mathbf{E}$, $\mathbf{B}$, $\mathbf{H}$, and $\mathbf{D}$. These equations are called the *constitutive relations*:

$$\mathbf{D}(\mathbf{r},\omega) = \epsilon_0[\boldsymbol{\epsilon}(z,\omega) \cdot \mathbf{E}(\mathbf{r},\omega) + \eta_0\boldsymbol{\xi}(z,\omega) \cdot \mathbf{H}(\mathbf{r},\omega)],$$
$$\mathbf{B}(\mathbf{r},\omega) = \frac{1}{c_0}[\boldsymbol{\zeta}(z,\omega) \cdot \mathbf{E}(\mathbf{r},\omega) + \eta_0\boldsymbol{\mu}(z,\omega) \cdot \mathbf{H}(\mathbf{r},\omega)], \quad \text{(A2)}$$

where $\mathbf{r} = x\hat{\mathbf{x}} + y\hat{\mathbf{y}} + z\hat{\mathbf{z}}$ and ω is the angular frequency. $\boldsymbol{\epsilon}$ and $\boldsymbol{\mu}$ are the *permittivity* dyadic and *permeability* dyadic of the medium, respectively, while $\boldsymbol{\xi}$ and $\boldsymbol{\zeta}$ are called crossed magnetoelectric dyadics. All four dyadics and all four fields can depend on the angular frequency ω, but this variable is suppressed below to simplify the notation.

In a single crystal, the physical and mechanical properties can often be orientation dependent. When the properties of a material vary with orientation, the material is said to be *anisotropic*. Alternatively, when the properties of a material are the same in all directions, the material is said to be *isotropic*. *Bi-anisotropic* is a general class of linear media which exhibit so-called magnetoelectric coupling between the electric and magnetic fields [8].

Based on the plane-stratified assumption, it is natural to decompose the electromagnetic field into tangential (x-y plane) and normal components. Considering the lateral homogeneity and substituting the constitutive relations (A2) into Maxwell's equations (A1) gives a system of ordinary differential equations (ODEs) with the variable z:

$$\frac{d}{dz}\begin{pmatrix} \mathbf{E}_{xy}(z) \\ \eta_0\mathbf{J} \cdot \mathbf{H}_{xy}(z) \end{pmatrix} = ik_0\mathbf{M}(z) \cdot \begin{pmatrix} \mathbf{E}_{xy}(z) \\ \eta_0\mathbf{J} \cdot \mathbf{H}_{xy}(z) \end{pmatrix}, \quad \text{(A3)}$$

where $\mathbf{J}$ is a two-dimensional rotation dyadic (rotation of $90°$ in the x-y plane) as follows:

$$\mathbf{J} = \begin{pmatrix} 0 & -1 \\ 1 & 0 \end{pmatrix} \quad \text{(A4)}$$

and

$$\mathbf{J} \cdot \mathbf{J} = -\mathbf{I}_2 = \begin{pmatrix} -1 & 0 \\ 0 & -1 \end{pmatrix}. \quad \text{(A5)}$$

For a more detailed discussion of how to obtain (A3), which is beyond the scope of this paper, the reader is referred to Ref. [8].

According to the main assumption, the plane-stratified media assumption, the four dyadics $\boldsymbol{\epsilon}(z), \boldsymbol{\xi}(z), \boldsymbol{\zeta}(z)$, and $\boldsymbol{\mu}(z)$ in (A2) depend only on one spatial variable z, which describes the propagation distance. The $Pr^{3+} : Y_2SiO_5$ crystal, which is our medium, is appropriately modeled as a nonmagnetic anisotropic medium with zero crossed magnetoelectric

dyadics. Therefore, as a second assumption, we assume nonmagnetic properties ($\mu = \mathbf{I}$) and also no crossed magnetoelectric dyadics ($\xi = \zeta = 0$) in (A2). There exists a general set of equations for the connection between the fundamental matrix $\mathbf{M}(z)$ and the four main dyadics in Ref. [8], but based on the three assumptions described above and a normal incident we can simplify $\mathbf{M}(z) = \mathbf{M}$ for our case as

$$\mathbf{M} = \begin{pmatrix} \bar{\bar{\mathbf{0}}} & -\bar{\bar{\mathbf{I}}}_2 \\ -\bar{\bar{\epsilon}}_{\perp\perp} + \frac{1}{\epsilon_{zz}}\bar{\epsilon}_\perp \bar{\epsilon}_z & \bar{\bar{\mathbf{0}}} \end{pmatrix}, \qquad \text{(A6)}$$

where

$$\bar{\bar{\epsilon}}_{\perp\perp} = \begin{pmatrix} \epsilon_{xx} & \epsilon_{xy} \\ \epsilon_{yx} & \epsilon_{yy} \end{pmatrix}, \quad \bar{\epsilon}_\perp = \begin{pmatrix} \epsilon_{xz} \\ \epsilon_{yz} \end{pmatrix},$$

$$\bar{\epsilon}_z = \begin{pmatrix} \epsilon_{zx} & \epsilon_{zy} \end{pmatrix}, \quad \bar{\bar{\mathbf{I}}}_2 = \begin{pmatrix} 1 & 0 \\ 0 & 1 \end{pmatrix}. \qquad \text{(A7)}$$

2. M tensor eigenvalues and eigenvectors

Following (A3) we need to investigate the eigenvalues and eigenvectors of the $\mathbf{M}$ tensor (A6) in order to calculate the tangential components of the electric and magnetic field. The eigenvectors $\mathbf{u}_i$ and $\mathbf{v}_i$ correspond to the eigenvalues $+\lambda_i$ and $-\lambda_i$ ($i = 1,2$) for the forward and backward waves, respectively,

$$\mathbf{u}_i = \{E_{ix}, E_{iy}, -\eta_0 H_{iy}, \eta_0 H_{ix}\}$$
$$\hspace{3cm} \text{for } i = 1,2.$$
$$\mathbf{v}_i = \{-E_{ix}, -E_{iy}, -\eta_0 H_{iy}, \eta_0 H_{ix}\}$$
$$\hspace{6cm} \text{(A8)}$$

For a full analytical derivation of the eigenvalues and eigenvectors see Appendix B.

3. E-field evolution in the propagation direction

To understand the $\mathbf{E}$-field and $\mathbf{H}$-field properties while the wave is propagating in the z direction, we can employ the fundamental equation for one-dimensional wave propagation (A3). By considering the eigenvectors and eigenvalues of the $\mathbf{M}$ matrix (A8), the wave properties along the propagation direction (z) is calculated for the forward wave:

$$\frac{d}{dz}\mathbf{u}_i = ik_0\lambda_i \mathbf{u}_i \implies \mathbf{u}_i(z) = \mathbf{u}_i(0)e^{ik_0\lambda_i z}. \qquad \text{(A9)}$$

It is possible to calculate the backward wave $\mathbf{v}_i(z)$ in the same way.

By convention, the polarization of light is described by specifying the orientation of the wave's electric field at a point in space over one period of the oscillation. Therefore, to understand the polarization direction inside the medium it is enough to only derive the $\mathbf{E}$ field. The initial light polarization before interaction with the medium could be described by the $\mathbf{E}$ field:

$$\mathbf{E}_0 = E_{0x}\hat{\mathbf{x}} + E_{0y}\hat{\mathbf{y}}. \qquad \text{(A10)}$$

In addition, the transverse electric field (x-y components) inside the medium could be written as a sum of the $\mathbf{E}$ field of the two eigenvectors:

$$\mathbf{E}_{\text{inside}} = A\mathbf{E}_1(z) + B\mathbf{E}_2(z)$$
$$= A(E_{1x}\hat{\mathbf{x}} + E_{1y}\hat{\mathbf{y}}) + B(E_{2x}\hat{\mathbf{x}} + E_{2y}\hat{\mathbf{y}}). \quad \text{(A11)}$$

Based on the boundary condition for the tangential $\mathbf{E}$ fields at the interface:

$$\hat{\mathbf{x}}: E_{0x} = AE_{1x} + BE_{2x}, \quad \hat{\mathbf{y}}: E_{0y} = AE_{1y} + BE_{2y}. \quad \text{(A12)}$$

Therefore,

$$A = \frac{E_{0x}E_{2y} - E_{0y}E_{2x}}{E_{1x}E_{2y} - E_{1y}E_{2x}}, \quad B = \frac{1}{E_{2x}}[E_{0x} - AE_{1x}]. \quad \text{(A13)}$$

Now we can extend our fields to a different z using (A9), (A11), and (A13) as follows:

$$\mathbf{u}(z) = A\mathbf{u}_1 e^{ik_0\lambda_1 z} + B\mathbf{u}_2 e^{ik_0\lambda_2 z}. \qquad \text{(A14)}$$

Note that since the $\mathbf{M}$ matrix does not depend on z in this case the eigenvalues and eigenvectors $+\lambda_i$, $-\lambda_i$, $\mathbf{u}_i$, and $\mathbf{v}_i$ remain constant and it is therefore possible to propagate the fields [or equivalently $\mathbf{u}(z)$ in (A14)] to any desired length in one step. In the more general case where the eigenvalues and eigenvectors changes with z one has to recalculate these in the simulations every distance Δz to be able to propagate the fields to z, where Δz is chosen for numerical stability and resolution.

Note also that the two polarization steady states for a forward propagating wave discussed in the main text is simply $\mathbf{u}_1$ and $\mathbf{u}_2$ where the solution with the lowest imaginary part of its eigenvalue is the stable solution while the other is the unstable solution. This can be understood since a high absorption leads to a fast decay from that state, i.e., the highest absorption gives the unstable state. In the same way, a large negative imaginary part corresponding to a high gain will generate a large component and therefore become stable since the other component can be neglected.

4. Light propagation in a $Pr^{3+} : Y_2SiO_5$ crystal

We start by calculating the permittivity tensor for $Pr^{3+} : Y_2SiO_5$ and then employ the theoretical approach discussed above to obtain the light polarization direction while propagating through this specific medium.

To define the permittivity tensor for $Pr^{3+} : Y_2SiO_5$ one could start by deriving the relation between permittivity and susceptibility for the host material (Y_2SiO_5) and the absorber (Pr) separately as follows:

$$\epsilon = (1 + \chi) = (1 + \chi_{\text{host}} + i\chi_{\text{abs}}). \qquad \text{(A15)}$$

The imaginary part of the susceptibility is proportional to the absorption, while the real part of the susceptibility is proportional to the real refractive index.

In Appendix B a full analytical derivation of the electric susceptibility χ_{abs} and the transition dipole moment angle θ is given but the following equations (A16) and (A17) are approximately correct for the case of $Pr^{3+} : Y_2SiO_5$.

χ_{abs} is a dimensionless quantity which represents the imaginary part of the electric susceptibility and is approximately proportional to the absorption coefficients ($\alpha_{D_1} + \alpha_{D_2}$), in the medium as follows [14]:

$$\chi_{\text{abs}} = \frac{n_{\text{bg}}c_0}{\omega}(\alpha_{D_1} + \alpha_{D_2}), \qquad \text{(A16)}$$

where $n_{\text{bg}} \approx 1.8$ is a background refractive index and $\omega \approx 2\pi \cdot 494 \times 10^{12}$ rad/s.

The anisotropic absorption coefficients for the two sites of a nominally 0.05% Pr^{3+} : Y_2SiO_5 crystal at the $^3H_4$ - $^1D_2$ transition is measured as shown in Table 7.6 in Ref. [11]. Based on this measurement the absorption for site I (605.977 nm) is about 3.6 ± 0.5 along the D_1, 47 ± 5 along the D_2, and <0.1 along the b axis, all in the unit cm^{-1} [see Fig. 2(a), where D_1, D_2, and b are crystal principal axes]. To estimate the susceptibility and the transition dipole moment angle θ, (A16) and the following equation are used (for more correct values see (B18);

$$\tan(\theta)^2 = \frac{\alpha_{D_2}}{\alpha_{D_1}},$$

$$\Rightarrow \theta = 74.5 \pm 1.9°, \qquad (A17)$$

$$\Rightarrow \chi_{abs} = (8.8 \pm 1.0) \times 10^{-4},$$

where χ_{abs} is given in the direction of the transition dipole moment shown in Fig. 2(a). It can be rotated about the b axis

to the principal axis coordinate system to be able to perform the summation in (A15):

$$\chi_{abs}^{crystal} = \mathbf{R_z}^{-1} \cdot \chi_{abs}^{dipole} \cdot \mathbf{R_z}$$

$$= \chi_{abs} \begin{pmatrix} \cos^2\theta & \sin\theta\cos\theta & 0 \\ \sin\theta\cos\theta & \sin^2\theta & 0 \\ 0 & 0 & 0 \end{pmatrix}. \quad (A18)$$

The next step is to calculate χ_{host} based on the Sellmeier dispersion and the measured coefficients from Table 7.1 and Eq. 7.2 in Ref. [11]:

$$\chi_{host} = \begin{pmatrix} 2.1973 & 0 & 0 \\ 0 & 2.2726 & 0 \\ 0 & 0 & 2.1867 \end{pmatrix}. \quad (A19)$$

Adding up all calculations, the final results for the permittivity tensor in the principal axis coordinate will be

$$\epsilon = \begin{pmatrix} \epsilon_{xx} & \epsilon_{xy} & \epsilon_{xz} \\ \epsilon_{yx} & \epsilon_{yy} & \epsilon_{yz} \\ \epsilon_{zx} & \epsilon_{zy} & \epsilon_{zz} \end{pmatrix} \qquad (A20)$$

$$= \begin{pmatrix} 1 + \chi_{xx} + i\chi_{abs}\cos^2\theta & i\chi_{abs}\sin\theta\cos\theta & 0 \\ i\chi_{abs}\sin\theta\cos\theta & 1 + \chi_{yy} + i\chi_{abs}\sin^2\theta & 0 \\ 0 & 0 & 1 + \chi_{zz} \end{pmatrix} \qquad (A21)$$

$$= \begin{pmatrix} 3.1973 + 6.2e^{-5}i & 2.3e^{-4}i & 0 \\ 2.3e^{-4}i & 3.2726 + 8.2e^{-4}i & 0 \\ 0 & 0 & 3.1867 \end{pmatrix}. \qquad (A22)$$

Using this permittivity tensor together with (A6), (A8), (A13), and (A14) it is possible to propagate light through an absorbing Pr^{3+} : Y_2SiO_5 crystal. Normally one can diagonalize a symmetric matrix by rotating the coordinate axes, this is however only possible for a real-valued matrix and not for a general complex symmetric matrix containing imaginary parts corresponding to losses or gain.

APPENDIX B: THEORETICAL ANALYSIS OF THE MATERIAL MATRIX M

For light propagating parallel to one crystal axis of a plane-stratified, nonmagnetic birefringent crystal with an absorption (or gain) axis in the transverse x-y plane and no crossed magnetoelectrical properties the material matrix **M** can be written as

$$\mathbf{M} = \begin{pmatrix} 0 & 0 & -1 & 0 \\ 0 & 0 & 0 & -1 \\ -n_{(D_1)}^2 - i\chi_{abs}\cos^2\theta & -i\chi_{abs}\cos\theta\sin\theta & 0 & 0 \\ -i\chi_{abs}\cos\theta\sin\theta & -n_{(D_2)}^2 - i\chi_{abs}\sin^2\theta & 0 & 0 \end{pmatrix}, \qquad (B1)$$

where $n_{(D_1)}$ and $n_{(D_2)}$ are the refractive indices of the two crystal axes in the x-y plane. θ is the angle from D_1 to the transition dipole moment axis and χ_{abs} is the electric susceptibility associated with the absorption.

The polarization steady states are given by the eigenvectors to the material matrix **M**. Four eigenvectors and eigenvalues exists and two of the eigenvalues have a positive real part which means they are connected to a forward traveling wave. These eigenvalues and eigenvectors are most important for the analysis in this paper. The stable eigenvector is the one whose eigenvalue has the lowest imaginary part (which is true for both positive imaginary parts in the case of absorption and for negative imaginary part in the case of gain).

Solving for the eigenvalues of **M** gives four eigenvalues:

$$\lambda_i = \pm \left[\frac{n_{(D_1)}^2 + n_{(D_2)}^2 + i\chi_{abs}}{2} \mp \frac{\chi_{abs}}{2} \sqrt{\left(\frac{n_{(D_2)}^2 - n_{(D_1)}^2}{\chi_{abs}} \right)^2 - 2i(1 - 2\sin^2\theta)\frac{n_{(D_2)}^2 - n_{(D_1)}^2}{\chi_{abs}} - 1} \right]^{1/2}. \qquad (B2)$$

Since we are only interested in the forward propagating waves only the eigenvalues whose real part is positive are of interest. These eigenvalues are denoted λ_1 and λ_2.

Before we solve for the eigenvectors in the general case we have to account for some special cases where $\theta = 0°$ or $\theta = 90°$. In these cases the transition dipole moment axis is parallel to one of the crystal axes D_1 or D_2 which of course results in two steady states, one along D_1 and another along D_2. Another special case is when the absorption is zero, which again is a trivial case where the polarizations of the steady states lie along D_1 and D_2.

Now that these special cases have been solved we will solve for the eigenvectors in the general case where we exclude the special cases mentioned above. The forward eigenvectors will be called $\mathbf{u}_i$:

$$\mathbf{u}_i = \{E_{ix}, E_{iy}, -\eta_0 H_{iy}, \eta_0 H_{ix}\} \tag{B3}$$

and the propagation is given by

$$\mathbf{u}_1(z) = \mathbf{u}_1(0)e^{ik_0\lambda_1 z}, \quad \mathbf{u}_2(z) = \mathbf{u}_2(0)e^{ik_0\lambda_2 z}. \tag{B4}$$

The eigenvector equations we want to solve are

$$\begin{pmatrix} 0 & 0 & -1 & 0 \\ 0 & 0 & 0 & -1 \\ -n_{(D_1)}^2 - i\chi_{\text{abs}}\cos^2\theta & -i\chi_{\text{abs}}\cos\theta\sin\theta & 0 & 0 \\ -i\chi_{\text{abs}}\cos\theta\sin\theta & -n_{(D_2)}^2 - i\chi_{\text{abs}}\sin^2\theta & 0 & 0 \end{pmatrix} \begin{pmatrix} E_{ix} \\ E_{iy} \\ -\eta_0 H_{iy} \\ \eta_0 H_{ix} \end{pmatrix} = \lambda_i \begin{pmatrix} E_{ix} \\ E_{iy} \\ -\eta_0 H_{iy} \\ \eta_0 H_{ix} \end{pmatrix}. \tag{B5}$$

The first two equations provides a relationship between the electric and magnetic fields and are omitted here since we are only interested in the ratio between the D_1 and D_2 components of the electric field to get the steady state solution, i.e., we only have to solve for the first two components of the eigenvector. This leaves us with two equations:

$$\left(n_{(D_1)}^2 + i\chi_{\text{abs}}\cos^2\theta\right)E_{ix} + (i\chi_{\text{abs}}\cos\theta\sin\theta)E_{iy} = \lambda_i^2 E_{ix}, \quad (i\chi_{\text{abs}}\cos\theta\sin\theta)E_{ix} + \left(n_{(D_2)}^2 + i\chi_{\text{abs}}\sin^2\theta\right)E_{iy} = \lambda_i^2 E_{iy}. \tag{B6}$$

Since we have the option to normalize the eigenvector in any way we set $E_{iy} = 1$ (assuming that $E_{iy} \neq 0$). Now solving for the ratio E_{ix}/E_{iy} we get

$$E_{ix} = \frac{E_{ix}}{E_{iy}} = \frac{i\chi_{\text{abs}}\cos\theta\sin\theta}{\lambda_i^2 - \left(n_{(D_1)}^2 + i\chi_{\text{abs}}\cos^2\theta\right)}. \tag{B7}$$

Using the following ratio:

$$R = \frac{n_{(D_2)}^2 - n_{(D_1)}^2}{\chi_{\text{abs}}}, \tag{B8}$$

Eq. (B7) [with λ_i from (B2)] can be rewritten in the following way:

$$\frac{E_{ix}}{E_{iy}} = \frac{2\cos\theta\sin\theta}{1 - 2\cos^2\theta - iR \mp \sqrt{1 - (1 - 2\sin^2\theta)^2 + [iR + (1 - 2\sin^2\theta)]^2}}. \tag{B9}$$

It can be shown that $\frac{E_{1x}}{E_{1y}} = -\frac{E_{2y}}{E_{2x}}$, which means that the two steady state solutions only differ by a $90°$ rotation in the D_1-D_2 plane since the two-dimensional rotation matrix for an angle of $90°$ is

$$\mathbf{J} = \begin{pmatrix} 0 & -1 \\ 1 & 0 \end{pmatrix}. \tag{B10}$$

1. Analysis when $R \to 0$

We can now solve for the steady state solutions (i.e., electric field components of the eigenvectors $\mathbf{u}_i$) in the limit $R \to 0$, which in other words means that the absorption is high compared to the phase retardation [see (3)]. The eigenvalues become

$$\lambda_1 \approx \sqrt{\frac{n_{(D_1)}^2 + n_{(D_2)}^2}{2}}, \quad \lambda_2 \approx \sqrt{\frac{n_{(D_1)}^2 + n_{(D_2)}^2}{2} + i\chi_{\text{abs}}}, \tag{B11}$$

i.e., one solution with no absorption (or gain) and a refractive index close to the refractive index of the material and one solution with high absorption (or gain) and a high refractive index.

The solution for the ratio of the electric field components becomes

$$\lambda_1 : \frac{E_{1x}}{E_{1y}} \approx -\tan(\theta), \quad \lambda_2 : \frac{E_{2x}}{E_{2y}} \approx \frac{1}{\tan\theta}. \tag{B12}$$

Since these are real numbers the polarizations are linear and the directions are for λ_2 along the transition dipole moment and for λ_1 perpendicular to it. Since the stable solution is the eigenvector whose eigenvalue has the lowest imaginary part, λ_1 is stable for absorption and λ_2 is stable for gain.

2. Analysis when $R \to \infty$

In the other limit where $R \to \infty$ the phase retardation dominates over the absorption which gives the following approximation of the eigenvalues:

$$\lambda_1 \approx \sqrt{n_{(D_1)}^2 + i\chi_{\text{abs}}\cos^2\theta}, \quad \lambda_2 \approx \sqrt{n_{(D_2)}^2 + i\chi_{\text{abs}}\sin^2\theta}. \tag{B13}$$

Here the stable solution depends on the transition dipole moment direction given by θ as well as the refractive indices $n_{(D_1)}$ and $n_{(D_2)}$. Using (B6) we can solve for the eigenvectors

in the limit when $R \to \infty$:

$$
\begin{aligned}
\lambda_1 \; : \; & \left(n_{(D_1)}^2 + i\chi_{\text{abs}}\cos^2\theta\right)E_{1x} + (i\chi_{\text{abs}}\cos\theta\sin\theta)E_{1y} \\
& \approx \left(n_{(D_1)}^2 + i\chi_{\text{abs}}\cos^2\theta\right)E_{1x} \\
& \Rightarrow E_{1y} \approx 0, \\
\lambda_2 \; : \; & (i\chi_{\text{abs}}\cos\theta\sin\theta)E_{2x} + \left(n_{(D_2)}^2 + i\chi_{\text{abs}}\sin^2\theta\right)E_{2y} \\
& \approx \left(n_{(D_2)}^2 + i\chi_{\text{abs}}\sin^2\theta\right)E_{2y} \\
& \Rightarrow E_{2x} \approx 0.
\end{aligned}
\tag{B14}
$$

From these equations it is clear that the eigenvector corresponding to λ_1 has almost no E_{1y} component and is therefore along D_1 and the reverse is true for λ_2.

3. Analysis of $Pr^{3+} : Y_2SiO_5$

In 0.05% $Pr^{3+} : Y_2SiO_5$ R is quite high so we can use the approximations made in the previous section for when $R \to \infty$. Continuing from (B13) we can write the imaginary part of λ_i as

$$
\begin{aligned}
\text{Im}(\lambda_1) &\approx \frac{1}{2}\sqrt{2\sqrt{n_{(D_1)}^4 + \chi_{\text{abs}}^2\cos^4\theta} - 2n_{(D_1)}^2}, \\
\text{Im}(\lambda_2) &\approx \frac{1}{2}\sqrt{2\sqrt{n_{(D_2)}^4 + \chi_{\text{abs}}^2\sin^4\theta} - 2n_{(D_2)}^2}.
\end{aligned}
\tag{B15}
$$

From these two equations we can solve for the transition dipole moment angle θ and the electric susceptibility associated with the absorption χ_{abs} to be

$$
\theta \approx \arctan\left[\left(\frac{\left\{2[\text{Im}(\lambda_2)]^2 + n_{(D_2)}^2\right\}^2 - n_{(D_2)}^4}{\left\{2[\text{Im}(\lambda_1)]^2 + n_{(D_1)}^2\right\}^2 - n_{(D_1)}^4}\right)^{1/4}\right],
$$

$$
\begin{aligned}
\chi_{\text{abs}} &\approx \sqrt{\left\{2[\text{Im}(\lambda_1)]^2 + n_{(D_1)}^2\right\}^2 - n_{(D_1)}^4} \\
&\quad + \sqrt{\left\{2[\text{Im}(\lambda_2)]^2 + n_{(D_2)}^2\right\}^2 - n_{(D_2)}^4}.
\end{aligned}
\tag{B16}
$$

In $Pr^{3+} : Y_2SiO_5$ the exponential decays of the intensity along D_1 and D_2 are measured and they are $\alpha_{D_1} = 3.6 \pm 0.5$ cm^{-1} and $\alpha_{D_2} = 47 \pm 5$ cm^{-1}, respectively. Given that the eigenvectors calculated in (B14) are along D_1 and D_2, respectively, one can, using (B4), write the following equation:

$$
\text{Im}(\lambda_1) = \frac{\alpha_{D_1}}{2k_0}, \quad \text{Im}(\lambda_2) = \frac{\alpha_{D_2}}{2k_0}, \quad k_0 = \frac{2\pi}{\lambda_0}, \tag{B17}
$$

where the factor of $1/2$ comes from that we now deal with electric fields and not intensities. k_0 is the wave number and λ_0 is the wavelength of the incoming wave in vacuum (not to be confused with λ_1 and λ_2 which are the eigenvalues of **M**). Using (B16) and (B17) one can calculate the angle θ from D_1 to the transition dipole moment axis and the absorption susceptibility χ_{abs} for a $Pr^{3+} : Y_2SiO_5$ crystal using $\lambda_0 = 605.977$ nm, $n_{(D_1)} = 1.7881$, and $n_{(D_2)} = 1.809$:

$$
\theta = 74.6 \pm 1.9°, \quad \chi_{\text{abs}} = (8.82 \pm 0.8) \times 10^{-4}. \tag{B18}
$$

An approximation of θ and χ_{abs} in (B16) can be made by assuming that $\text{Im}(\lambda_i) \ll n_{D_i}$ and that $n_{(D_1)} \approx n_{(D_2)} \approx n_{\text{bg}}$ (which is the case for $Pr^{3+} : Y_2SiO_5$). This results in

$$
\begin{aligned}
\theta &\approx \arctan\left(\left\{\frac{[\text{Im}(\lambda_2)]^2 n_{(D_2)}^2}{[\text{Im}(\lambda_1)]^2 n_{(D_1)}^2}\right\}^{1/4}\right) \\
&\approx \arctan\left(\sqrt{\frac{\text{Im}(\lambda_2)}{\text{Im}(\lambda_1)}}\right) = \arctan\left(\sqrt{\frac{\alpha_{D_2}}{\alpha_{D_1}}}\right)
\end{aligned}
\tag{B19}
$$

and

$$
\begin{aligned}
\chi_{\text{abs}} &\approx 2\text{Im}(\lambda_1)n_{(D_1)} + 2\text{Im}(\lambda_2)n_{(D_2)} \\
&= \frac{\alpha_{D_1}n_{(D_1)}}{k_0} + \frac{\alpha_{D_2}n_{(D_2)}}{k_0} \approx \frac{(\alpha_{D_1} + \alpha_{D_2})n_{\text{bg}}}{k_0}.
\end{aligned}
\tag{B20}
$$

Equations (B19) and (B20) are only valid in the case where $R \to \infty$ but allows us to use (A16) and (A17) for the case of $Pr^{3+} : Y_2SiO_5$ which gives values quite close to the more correct values obtained in (B18).

4. Continuation of analysis when $R \to 0$

In the other case where $R \to 0$ we only have one axis with absorption [see (B11)] and therefore in (B17) we replace α_{D_2} by α_{dipole} that measures the absorption along the transition dipole moment axis for λ_2 whose eigenvector points in that direction and set $\text{Im}(\lambda_1) = 0$. θ is now given by the angle from the crystal axis to the axis of which the absorption is measured. Assuming that $\chi_{\text{abs}} \gg n_{D_i}^2$ the following proportionality between χ_{abs} and α_{dipole} can also be calculated using (B11):

$$
\chi_{\text{abs}} \approx \frac{1}{2}\left(\frac{\alpha_{\text{dipole}}}{k_0}\right)^2. \tag{B21}
$$

This shows that the electric susceptibility χ_{abs} does not always scale linearly with the absorption coefficient α_{dipole}.

[1] B. E. A. Saleh and M. C. Teich, *Fundamentals of Photonics*, 2nd ed. (Wiley Series in Pure and Applied Optics, New York, 2007).

[2] M. J. F. Digonnet, Ed., *Rare-Earth-Doped Fiber Lasers and Amplifiers*, 2nd ed. (CRC, Boca Raton, FL, 2001).

[3] H. de Riedmatten and M. Afzelius, *Engineering the Atom-Photon Interaction* (Springer, New York, 2015), pp. 241–273, part of the series Nano-Optics and Nanophotonics.

[4] R. Winston, J. C. Miñano, and P. Benítez, contributed by N. Shatz and J. C. Bortz, *Nonimaging Optics* (Elsevier Academic Press, Burlington, MA, 2005).

[5] H. Zhang, M. Sabooni, L. Rippe, C. Kim, S. Kröll, L. V. Wang, and P. R. Hemmer, Appl. Phys. Lett. **100**, 131102 (2012).

[6] A. Louchet-Chauvet, R. Lauro, P. Goldner, F. Ramaz, T. Chaneliére, and J. L. Le Gouët, Adv. Photon. Quantum Comput. Memory Commun. IV **7948**, 794805 (2011).

[7] S. E. Beavan, E. A. Goldschmidt, and M. J. Sellars, J. Opt. Soc. Am. B **30**, 1173 (2013).

[8] S. Rikte, G. Kristensson, and M. Andersson, IEE Proc. Microw. Antennas Propag. **148**, 29 (2001).

[9] J.-X. Cheng and X. S. Xie, *Coherent Raman Scattering Microscopy* (CRC, Boca Raton, FL, 2012), pp. 65–69.

[10] R. P. Feynman, R. B. Leighton, and M. Sands, *The Feynman Lectures on Physics*, Vol. 1 (Addison-Wesley, Reading, MA, 1963), Sec. 30.7 (http://www.feynmanlectures.caltech.edu/).

[11] Y. C. Sun, *Spectroscopic Properties of Rare-Earths in Optical Materials*, edited by G. Liu and B. Jacquier (Springer Series in Material Science, New York, 2005), Chap. 7.

[12] R. Beach, M. D. Shinn, L. Davis, R. W. Solart, and W. F. Krupke, IEEE J. Quantum Electron. **26**, 1405 (1990).

[13] A. Walther, A. Amari, S. Kröll, and A. Kalachev, Phys. Rev. A **80**, 012317 (2009) (correction: the expression for the group velocity needs to be corrected to $v_g = \frac{2\pi\Gamma}{\alpha}$ in Sec. IV B).

[14] H. Haug and S. W. Koch, *Quantum Theory of the Optical and Electronic Properties of Semiconductors* (World Scientific, Singapore, 2004).